

Map-based E/B separation of filtered timestreams using space-based E-mode observations

Yuyang Zhou^a Adrian Lee^{a,b} Yuji Chinone^{c,d}

^aDepartment of Physics, University of California, Berkeley, Berkeley, CA 94720, USA

^bPhysics Division, Lawrence Berkeley National Laboratory, Berkeley, CA 94720, USA

^cInternational Center for Quantum-field Measurement Systems for Studies of the Universe and Particles (QUP), High Energy Accelerator Research Organization (KEK), Tsukuba, Ibaraki 305-0801, Japan

^dKavli Institute for the Physics and Mathematics of the Universe (WPI), UTIAS, The University of Tokyo, Kashiwa, Chiba 277-8583, Japan

E-mail: yuyang_zhou@berkeley.edu, Adrian.Lee@berkeley.edu, chinoney@gmail.com

Abstract. E to B mixing or “leakage” due to time-ordered data (TOD) filtering has become an important source of sensitivity loss that ground-based cosmic microwave background polarization experiments must address. However, it is a difficult problem for which very few viable solutions exist. In this paper, we expand upon satellite E-mode methods to cover E/B leakage specifically due to TOD filtering. We take a satellite E-mode map and TOD filter it through the ground-based experiment data analysis pipeline, from which we construct a map-space “leakage template” and subtract it from the ground-based experiment map. We evaluate the residual leakage by simulating the satellite E-mode maps with Planck-like and LiteBIRD-like noise levels, and simulate the ground-based experiment with Simons Observatory-like and CMB-S4-like noise levels. The effectiveness of the method is measured in the improvement of the Fisher uncertainty $\sigma(r = 0)$. We find that our method can reduce $\sigma(r = 0)$ by $\sim 15\text{--}75\%$ depending on the noise levels considered.

Contents

1	Introduction	1
2	E/B Mixing	3
2.1	E/B decomposition	3
2.2	Partial sky coverage	3
2.3	TOD filtering	4
2.4	Matrix purification	4
2.5	Map-based E/B separation	5
3	Simulations	7
3.1	Ground-based experiment analysis pipeline and noise simulations	7
3.2	Satellite E-mode map generation	10
3.3	Implementation: map-based E/B separation	12
4	Results	13
4.1	Leakage maps and spectra (TTEE input)	13
4.2	Spectra with noise and lensing residuals (TTEEBB input)	14
4.3	Fisher forecast for $\sigma(r = 0)$	15
5	Discussion	17
5.1	Future work	17
6	Conclusion	18
A	Implementation: matrix purification	18

1 Introduction

The cosmic microwave background (CMB) is our most powerful observational probe of physical conditions in the early universe. While its spectrum and temperature anisotropies have been exquisitely measured by numerous experiments [1–3], its polarization anisotropies remain a frontier waiting to be fully characterized. In particular, the B-mode component (defined in Section 2.1) is expected to contain the imprint of the stochastic background of gravitational waves predicted by theories of cosmic inflation [4]. The yet undetected amplitude of this signal depends sensitively on the energy scale of inflation, providing a powerful constraint on the space of inflationary models. A precise measurement of the primordial B-mode polarization thus lies at the forefront of modern cosmology.

As experiments get more sensitive in this pursuit, systematics previously buried underneath the noise spectrum start to become relevant. One such effect is the leaked E-mode variance into the B-mode spectrum due to time-domain filtering of the polarization time-ordered data (TOD), so called E-to-B (E/B) leakage. This occurs in ground-based experiments utilizing filter-bin mapmaking pipelines [5], which is the method of choice for large datasets [6]. Since E-modes are much brighter than the primordial B-mode signal, any leaked variance will dramatically affect the overall BB sensitivity.

In the past, ground-based experiments have handled E/B leakage due to TOD filtering by generating filtered TTEE simulations and subtracting the mean of the resulting BB leakage spectrum from the data BB spectrum (recent example in [7]). While this successfully debiases the data BB mean, it does not remove the variance of the much brighter E-modes, resulting in decreased BB sensitivity at low multipoles. For experiments achieving a map depth of below a few $\mu\text{K}\text{-arcmin}$, this effect will be dominant over the noise spectrum (Figure 1) and thus will need to be treated in a more sophisticated way.

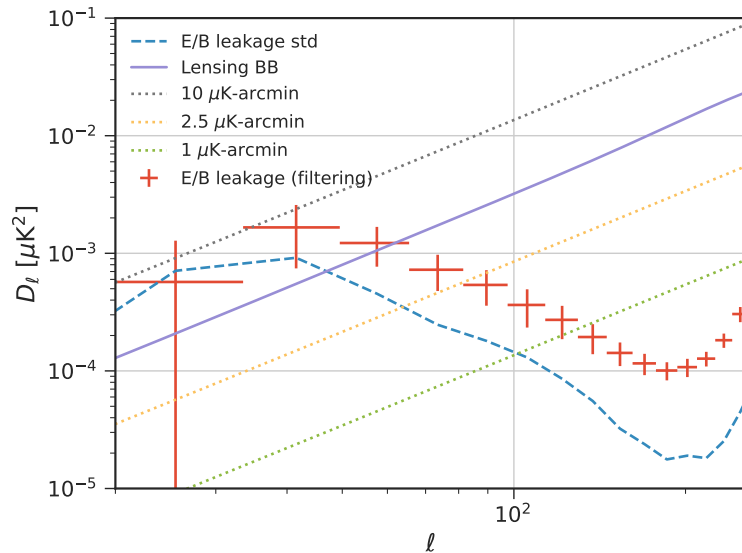


Figure 1. Comparison between the BB leakage spectra (red) due to TOD filtering and a few different white noise levels. The leakage spectra is estimated from filtering 128 TTEE maps with a standard subscan polynomial and ground template subtraction. The mean is plotted in each bin with standard deviation error bars with the standard deviation also plotted separately in the blue dashed line. We see that the leakage spectrum, concentrated at low- ℓ due to the nature of the filtering, becomes dominant over the noise spectra for more sensitive experiments.

To the best of our knowledge, the only successful demonstration of mitigating E/B leakage due to TOD filtering on a real dataset is that of “matrix purification,” a method implemented by the BICEP/Keck collaboration [8] at the South Pole. However, while effective, this method is computationally demanding and may prove to be challenging to implement for experiments with increasing detector count and Chilean scan strategies [9] (see discussion in Section 2.4). Nevertheless, the matrix purification approach is an avenue currently being explored for the Simons Observatory (SO) [10] based in Chile.

In this paper, we propose a simpler, less computationally demanding alternative by extending the work of [11]. We leverage a single, deep E-mode map with sufficient low- ℓ coverage (such as a space mission) and TOD filter it through the ground-based experiment data analysis pipeline to estimate a “leakage template” in map space. While the method presented in [11] mitigates E/B leakage due to partial-sky coverage (Section 2.2), our method extends this to cover E/B leakage due to TOD filtering (Section 2.3) for which no easily implementable solutions currently exist. To evaluate noise scaling, we simulate Planck [3] and LiteBIRD [12] noise levels for the satellite E-mode maps and SO and CMB-S4 (S4) [6] noise levels for the ground-based experiment maps. Finally, we forecast the improvement on

$\sigma(r)$ and compare the results to the existing matrix purification method.

2 E/B Mixing

2.1 E/B decomposition

Experiments measure CMB polarization in terms of the Stokes parameters Q/U, which are related to the underlying polarization field via the spin-2 spherical harmonics [13]

$$Q \pm iU = \sum_{l,m} \pm_2 a_{\ell m} \pm_2 Y_{l,m}. \quad (2.1)$$

Since Stokes Q/U depend on the coordinate system, power spectrum results are usually presented in the rotationally invariant basis, denoted E and B. The corresponding coefficients are defined as

$$\begin{aligned} a_{\ell m}^E &\equiv -({}_2a_{\ell m} + {}_{-2}a_{\ell m})/2 \\ a_{\ell m}^B &\equiv -i({}_2a_{\ell m} - {}_{-2}a_{\ell m})/2 \end{aligned} \quad (2.2)$$

and similarly the spherical harmonics (in vector notation)

$$\begin{aligned} Y_{\ell m}^E &\equiv \begin{pmatrix} ({}_2Y_{\ell m} + {}_{-2}Y_{\ell m})/2 \\ -i({}_2Y_{\ell m} - {}_{-2}Y_{\ell m})/2 \end{pmatrix} \\ Y_{\ell m}^B &\equiv \begin{pmatrix} i({}_2Y_{\ell m} - {}_{-2}Y_{\ell m})/2 \\ ({}_2Y_{\ell m} + {}_{-2}Y_{\ell m})/2 \end{pmatrix} \end{aligned} \quad (2.3)$$

with

$$\int_{S^2} Y_{\ell m}^E \cdot Y_{\ell' m'}^B dS = 0 \quad (2.4)$$

over the full sphere [8]. The overall polarization field can then be written as

$$\mathbf{P} = \begin{pmatrix} Q \\ U \end{pmatrix} = - \sum_{l,m} a_{\ell m}^E Y_{\ell m}^E + a_{\ell m}^B Y_{\ell m}^B. \quad (2.5)$$

where it is straightforward to see that E and B-only polarization fields are orthogonal over the full sky

$$\int_{S^2} \mathbf{P}^E \cdot \mathbf{P}^B dS = 0. \quad (2.6)$$

That is, there is no E/B mixing when we have a complete measurement of the sky signal.

When we do not have a complete measurement (i.e. information loss), we have E/B mixing. The two main sources relevant for ground-based experiments are partial-sky coverage and TOD filtering, in order of impact.

2.2 Partial sky coverage

Ground-based observatories naturally only have access to part of the sky, causing Equation 2.6 to be no longer integrated over the full sphere. In this case, the spaces of E and B-modes begin to mix, with the overlap comprising “ambiguous” modes, which contribute power to both EE and BB.

Techniques to deal with the E/B mixing due to partial sky coverage have been extensively studied, with the most widely-used being [14, 15], which we will refer to as “KS purification” after the author. For the simulation results in the rest of this paper, we make use of the NaMaster pseudo- C_ℓ package’s [16] implementation of KS purification.

2.3 TOD filtering

All ground-based experiments employ some form of TOD filtering to suppress low-frequency noise, such as the atmosphere, ground emission, and thermal drifts. Due to the scanning direction of the telescope, the filtering runs along a specific direction on the sky. This means that different $Y_{\ell m}$ modes are affected differently by the filtering depending on their orientation, breaking the orthogonality relation in Equation 2.6 and inducing E/B mixing. For Stage-2 experiments such as POLARBEAR [7] targeting $\sigma(r) \sim 10^{-2}$, the E/B leakage caused by TOD filtering was subdominant to the noise. Thus, only the mean level of leakage was estimated from filtered TTEE simulations and subtracted from the pseudospectra via

$$\tilde{C}_\ell^{E \rightarrow B} = \frac{F_\ell^{E \rightarrow B}}{F_\ell^{E \rightarrow E}} \tilde{C}_\ell^E \quad (2.7)$$

where F_ℓ is the filter transfer function approximated as the ratio of output over input power spectra. While this correctly debiases the central value of BB in each bin, the leaked variance of the E-modes is left in the data.

For Stage-3/4 experiments such as SO [10] and S4 [6] targeting $\sigma(r) \sim 10^{-3}$ and below, the leaked E-mode variance is now dominant over the noise spectrum, prompting the development of new techniques to deal with this now-relevant effect. The canonical solution has become the BICEP/Keck collaboration’s matrix purification method [8], which we briefly review in the next section.

2.4 Matrix purification

The method of matrix purification involves finding “pure-B” modes that remain orthogonal to the E-modes after pipeline processing (masking, filtering, etc.). We seek to construct a new basis that satisfies

$$\mathbf{R} \mathbf{P}^E \cdot \mathbf{b} = 0 \quad (2.8)$$

where \mathbf{R} is a linear operator called the “observation matrix” and \mathbf{b} is the new pure-B basis. \mathbf{R} represents the application of the entire data analysis pipeline, including data selection, filtering, apodization, etc. We will henceforth refer to maps processed through the pipeline onto a sky patch as “observed” maps. \mathbf{b} is constructed by solving the generalized eigenvalue problem (omitting the regularization factor for clutter)

$$\tilde{\mathbf{C}}_B \mathbf{x}_i = \lambda_i \tilde{\mathbf{C}}_E \mathbf{x}_i \quad (2.9)$$

where $\tilde{\mathbf{C}}_{E/B}$ are the “observed” signal covariances

$$\tilde{\mathbf{C}}_{E/B} = \mathbf{R}^\top \left(\sum_{l,m} C_\ell^{EE/BB} Y_{\ell m}^{E/B} Y_{\ell m}^{E/B\dagger} \right) \mathbf{R}. \quad (2.10)$$

The unobserved signal covariances inside the brackets above are generated analytically following Appendix A of [17]. The solved eigenvectors of Equation 2.9 form our new basis of pure-B modes \mathbf{b} , with the eigenvectors with larger eigenvalues being more “pure” than eigenvectors with smaller eigenvalues, since

$$\mathbf{b}^\top \tilde{\mathbf{C}}_B \mathbf{b} \gg \mathbf{b}^\top \tilde{\mathbf{C}}_E \mathbf{b}. \quad (2.11)$$

Lastly, a “purification” matrix is constructed via a projection operator using the pure-B basis

$$\mathbf{\Pi}_B = \sum_i \mathbf{b}_i (\mathbf{b}_i^\top \mathbf{b}_i)^{-1} \mathbf{b}_i^\top. \quad (2.12)$$

The application of $\mathbf{\Pi}_B$ to an observed map projects the map onto the space of pure-B modes

$$\mathbf{m}_{\text{purified}} = \mathbf{\Pi}_B \mathbf{m}_{\text{obs}} \quad (2.13)$$

thereby removing the B contribution of ambiguous modes and mitigating E/B leakage.

There are primarily two computational challenges associated with the matrix purification method. The first is the generation of the observation matrix, for which the computation time depends on a number of factors. A bare-bones simulation for the SO small aperture telescope (SAT)’s south patch running at a reduced resolution of $N_{\text{side}} = 128$ in the HEALPix¹ scheme, for 1/8 of the detectors in the 145 GHz band, with scanning taken from 10 operational days, using a simple subscan polyfilter and ground template subtraction, takes about 1 hour on 4 NERSC Perlmutter CPU nodes². While this may not sound prohibitive, there are several complicating factors. First, the computation time scales linearly with number of detectors and days of scanning. Second, it is important to preserve the sparsity of the observation matrix due to hardware memory limits. The minimal simulation above only uses a subscan polyfilter and ground template subtraction, resulting in about 5% density. Increasing to $N_{\text{side}} = 256$ at the same sparsity exceeds the 512 GB memory limit of a NERSC Perlmutter CPU node. On top of that, including additional filtering that target many detectors/long timescales (such as a common mode filter) radically destroys the sparsity, limiting the choice of the filter stack for more realistic scenarios. In any case, the large memory footprint of the observation matrix makes subsequent matrix operations cumbersome.

The second challenge is solving the generalized eigenvalue problem in Equation 2.9. For the implementation used in this paper at $N_{\text{side}} = 128$, `scipy.sparse.eigsh`³ takes around 30 hours to calculate 7250 eigenvectors on a local CPU cluster running Intel(R) Xeon(R) E5-2650 v4 with 48 logical cores. Despite each observed covariance matrix in Equation 2.10 being less than 3 GB, the routine required over 50 GB of memory to complete, hinting at exponentially larger memory allocations required for higher resolutions/density.

Lastly, any changes made to the pipeline (data selection, filtering, etc) means the process needs to be repeated all over again, making iteration computationally expensive. Given these complications, the feasibility of implementing matrix purification for SO is an ongoing area of study. The details of the implementation used in this paper is described in Appendix A.

2.5 Map-based E/B separation

Given the computational challenges of the matrix purification method, we now introduce an alternative map-based E/B separation approach based on [11]. We describe the basic procedure in this section and leave the details of the implementation for Section 3.

The main idea is as follows: given a perfect, noiseless map of the E-modes, E/B mixing would be essentially solved. We could process the map through any arbitrary data analysis pipeline, get the resulting B-mode leakage map, and remove it from our data. In contrast to the method described in Equation 2.7, this removes the leakage in map space as opposed to power spectrum space, which retains the full anisotropic information of the data.

¹<https://healpix.sourceforge.io/>

²<https://docs.nersc.gov/systems/perlmutter/architecture/>

³<https://docs.scipy.org/doc/scipy/reference/generated/scipy.sparse.linalg.eigsh.html>

While a perfect E-mode map may never exist, we can nevertheless try to approximate this method by using existing noisy E-mode maps with sufficient low- ℓ coverage. One good candidate available to us now would be the Planck satellite [3] E-modes, or in the future the LiteBIRD satellite [12] E-modes. With increasing noise levels of the satellite E-modes, our ability to estimate the E/B leakage template diminishes. The simulations in this paper aim to study the relationship between the satellite E-mode noise level and its effect on removing the E/B leakage incurred by TOD filtering. We simulate Planck-like and LiteBIRD-like noise levels for the satellite E-mode map and see if the residual leakage still dominates the sensitivity loss, as well as taking into account the ground-based experiment map depth. See Figure 2 for flowchart of the procedure.

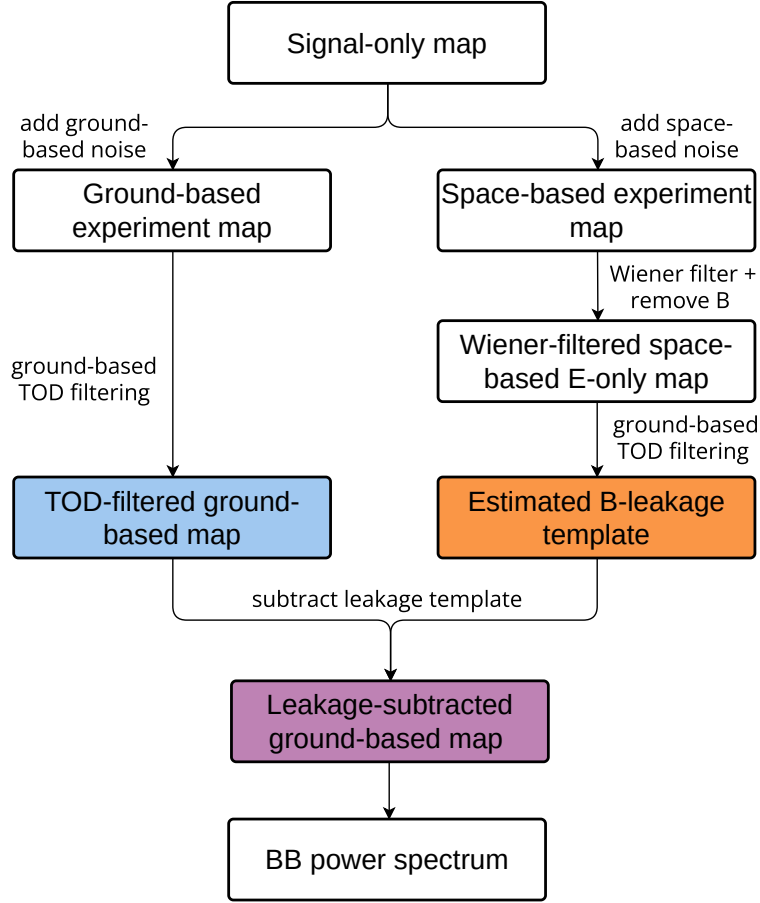


Figure 2. Flowchart illustrating the process of map-based E/B separation. From a signal-only input map, we construct a ground-based experiment map with ground-based experiment noise and an E-mode only map with satellite experiment noise. The E-mode map is filtered through the same pipeline as the ground-based experiment, and the resulting B-mode map is used as a template for leakage removal. This process is repeated for each Monte Carlo (MC) simulation.

Conceptually, the method is simple, which is a strength. Computationally, it would only require one additional run of the data analysis pipeline, which is trivial. It can also be done at any N_{side} without incurring cascading computational resources, unlike the matrix purification method. In the next section, we describe the simulation framework in more detail.

3 Simulations

The simulation pipeline used to generate the results is made of four parts corresponding to Figure 2:

1. Λ CDM signal-only maps
2. Ground-based experiment analysis pipeline + noise simulations
3. Satellite E-mode maps with isotropic noise
4. Power spectrum estimator

For 1. Λ CDM signal-only maps, we use the `healpy.sphtfunc.synfast`⁴ with default Planck 2018 parameters⁵. For the sake of simplicity, all maps are binned at $N_{\text{side}} = 128$ with smoothing based on pixel size, which ends up being roughly equivalent to a beam FWHM (θ_{fwhm}) of $\approx 1^\circ$. Since we are mostly interested in studying the filtering leakage which manifests at low- ℓ , this resolution is sufficient. In practice, maps from different experiments will need to be smoothed to a common beam before being combined. All simulations labeled “TTEE/TTBB/TTEEBB” use Λ CDM input unless otherwise specified.

For 4. Power spectrum estimator, we use the NaMaster package [16] to debias our pseudospectra and apply KS purification (for partial-sky leakage). The maps are apodized on the scale of 10° in the “C2” scheme. All debiased spectra shown are binned at $\Delta\ell=16$.

Items 2 and 3 will be discussed in further detail below.

3.1 Ground-based experiment analysis pipeline and noise simulations

We construct a simple filter-bin pipeline to simulate our ground-based experiment maps, using the Time Ordered Astrophysics Scalable Tools (TOAST) ver. 3 software package [18]. All steps below are easily supported using built-in TOAST pipeline tools.

First, we generate a short 24-hour observing schedule at the Chilean Cerro Toco site targeting part of the southern field between $15 < \text{RA} < 65$ and $-50 < \text{DEC} < -30$. This covers about 4.4% of the sky, compared to the S4 deep patch (3%) [6] and the SO SAT patch (10%) [10]. The observing schedule is able to scan the patch twice a day with constant elevation scans (CES) at different azimuths, enabling cross-linking. Figure 3 shows the hit map for a simulated focal plane with a small number of detectors.

The chosen filter stack is an order 1 polynomial subtraction for each subscan (CES between turnarounds) and an order 10 Legendre polynomial ground template (scan-synchronous signal) subtraction for the Q/U polarization TODs. These are standard filters that all ground-based experiments incorporate in some form and are known to cause E/B leakage due to their anisotropic nature. See Figure 4 for a visual example of the filtering.

The BB filter transfer function F_ℓ is estimated iteratively with TTBB signal-only simulations, following [5]

$$F_\ell^n = F_\ell^{n-1} + \frac{\tilde{C}_\ell - \sum_{\ell'} \mathbf{M}_{\ell\ell'} F_\ell^{n-1} C_{\ell'} B_{\ell'}^2}{C_\ell B_\ell^2 f_{\text{sky}} w_2}, F_\ell^0 = \mathbf{1} \quad (3.1)$$

where \tilde{C}_ℓ is the simulated pseudospectra, $\mathbf{M}_{\ell\ell'}$ is the mode mixing matrix, B_ℓ is the Gaussian beam function (with $\theta_{\text{fwhm}} \approx 1^\circ$), and w_2 is the second moment of the weight function. We

⁴<https://healpy.readthedocs.io/en/latest/generated/healpy.sphtfunc.synfast.html>

⁵https://github.com/cmbant/CAMB/blob/master/inifiles/planck_2018.ini

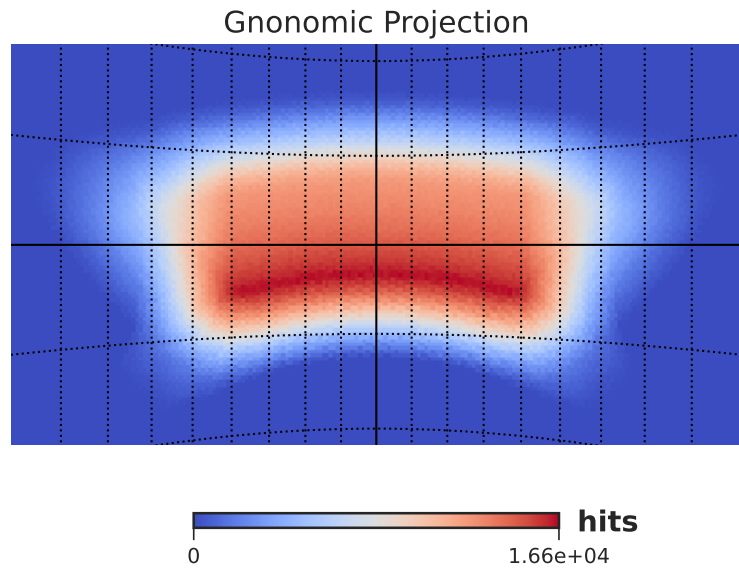


Figure 3. Simulated ground-based experiment hit map over a 24 hour period. Covers a sky fraction of about 4.4% in the southern field.

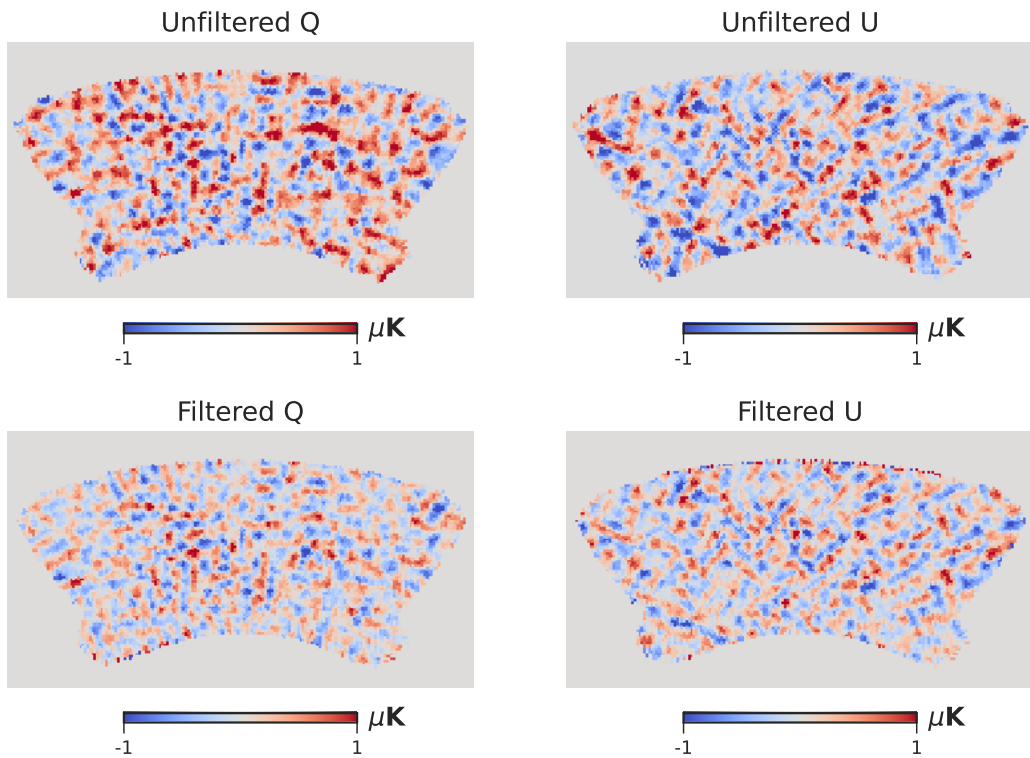


Figure 4. Filtered vs unfiltered Stokes Q/U for a single signal-only TTEEBB realization. The filtering removes power on large scales, creating the “washed out” effect seen in these maps.

find 3 iterations gives stable results and use it to debias subsequent pseudospectra. Note that while not explicitly written in Equation 3.1, we count the purification processes as part of the filtering, resulting in slightly different transfer functions for KS and matrix purifications (Figure 5).

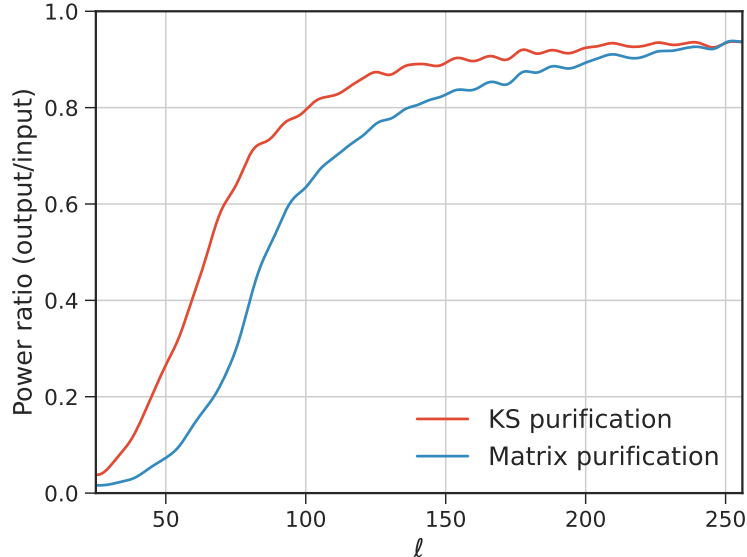


Figure 5. The filter transfer function including KS and matrix purifications estimated from the mean of 1024 TTBB signal-only simulations. The filtering removes large scale power, reaching about 50% signal attenuation around $\ell = 60$ for KS purification. The matrix purification filter transfer function is lower in magnitude due to the removal of power from ambiguous modes.

The noise generation comprises an atmospheric noise simulation as well as a detector noise portion. The spectral properties (NET , f_{knee} , α) are adjusted to achieve a desired final map depth in polarization. We simulate two different map depths for the same patch in Figure 3 to approximate the noise spectra in Table 1, allowing us to evaluate our E/B separation methods in the context of BB noise. The noise spectra N_ℓ follows the usual definition (without the beam)

$$N_\ell = N_w + N_w \left(\frac{\ell}{\ell_{\text{knee}}} \right)^\alpha \quad (3.2)$$

with N_w being the white noise level set by the map depth. No correlated noise among detectors is simulated. See Figure 6 for an example noise realization.

	Map depth ($\mu\text{K-arcmin}$)	ℓ_{knee}	α
“SO-like” pol	3	50	-3
“S4-like” pol	1	50	-3

Table 1. We simulate two different map depths in polarization for the ground-based experiment, one SO-like [10] depth and one S4-like [6] depth.

While our ground-based experiment simulations approximate SO and S4 SAT map depths, we emphasize that the results in this paper are not meant to be a realistic forecast of

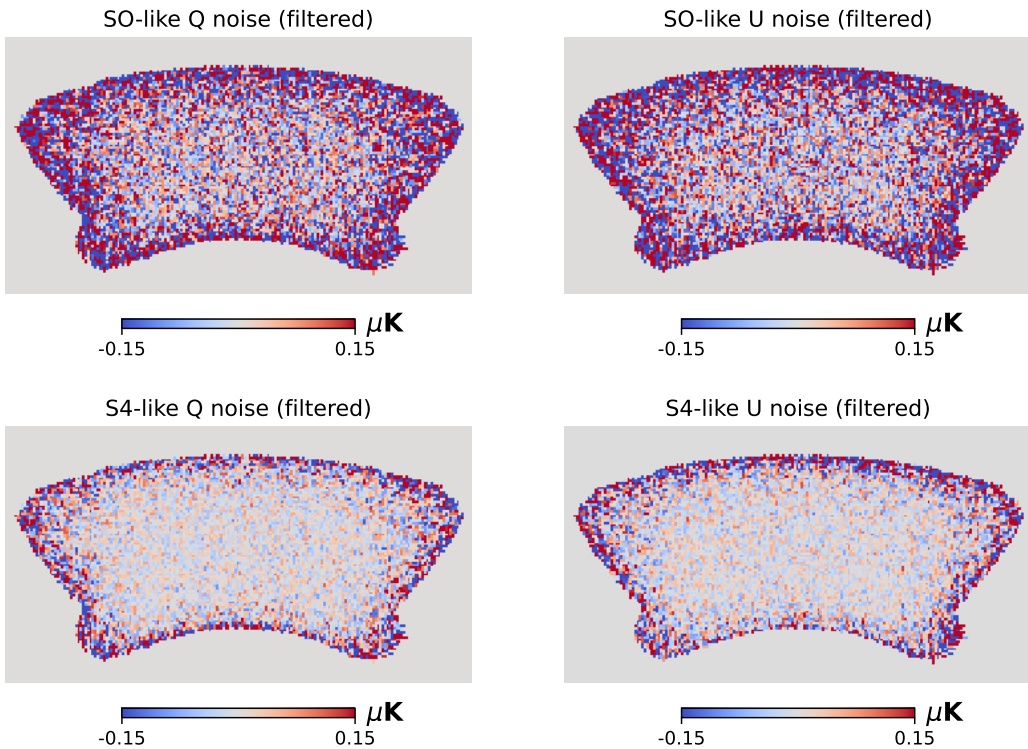


Figure 6. Example simulated Q/U noise maps (filtered) of the SO-like and S4-like simulations, same color scale. The edges of the map are higher in noise due to the scanning coverage.

the aforementioned experiments. For example, our observing patch matches that of neither experiment, and mostly serves as a generic setup that allows us to simulate different map depths while keeping everything else equal.

The final, filter-binned ground-based experiment map for each Monte Carlo (MC) simulation is taken to be the sum of the observed signal-only map and the simulated noise map in Figure 6.

3.2 Satellite E-mode map generation

To generate a full-sky E-mode map with noise, we use `healpy.sphtfunc.synfast` to generate isotropic noise and add it to the original signal-only map. As with the ground-based experiment, we simulate two different noise levels for the satellite E-modes (Table 2).

We note that while we chose map depths of the satellite E-modes to be similar to that of Planck and LiteBIRD, we reiterate that this study is not representative of a comprehensive forecast associated with either experiment.

Before we estimate the leakage template, we apply a multivariate Wiener filter to the noisy satellite E-mode map to obtain a minimum variance solution following [11]. This is especially important for the noisier Planck-like E-modes, so we do not overestimate the leakage template. We have

$$\mathbf{W} = \mathbf{S}(\mathbf{S} + \mathbf{N})^{-1} = \begin{pmatrix} W_{\ell}^{TT} & W_{\ell}^{TE} \\ W_{\ell}^{ET} & W_{\ell}^{EE} \end{pmatrix} \quad (3.3)$$

	Map depth ($\mu\text{K-arcmin}$)	ℓ_{knee}	α
“Planck-like” temp	25	50	-1.8
“Planck-like” pol	50	25	-1.4
“LiteBIRD-like” temp	1.8	-	-
“LiteBIRD-like” pol	2.16	-	-

Table 2. Noise spectra parameters added to the satellite E-mode maps. Both temperature and polarization noise are simulated for the Wiener filtering step discussed below. The Planck-like values are estimated from the NPIPE2020 maps: <https://portal.nersc.gov/project/cmb/planck2020/>. The LiteBIRD-like values [12] assume white noise only due to the half-wave plate effectively eliminating the ℓ_{knee} . The map depth in temperature is simply scaled to be a $\sqrt{2}$ factor smaller than the polarization for simplicity — it is inconsequential if LiteBIRD actually makes a temperature measurement.

where \mathbf{S} is the 2×2 TTEE beam-convolved input signal power spectra and \mathbf{N} is the 2×2 TTEE noise power spectra that was simulated with the spectral properties in Table 2. The Wiener-filtered E-mode spherical harmonic coefficients are then

$$\widehat{d}_{\ell m}^E = W_{\ell}^{ET} d_{\ell m}^T + W_{\ell}^{EE} d_{\ell m}^E \quad (3.4)$$

where $d_{\ell m}^{T/E}$ are the spherical harmonic coefficients of the noisy map and $d_{\ell m}^B$ is set to zero. Including the temperature measurement recovers a significant amount of signal for the Planck-like case. $\widehat{d}_{\ell m}^E$ is then transformed back into Q/U space to use as our final satellite E-mode map. Figure 7 and Figure 8 show the Wiener filter in action.

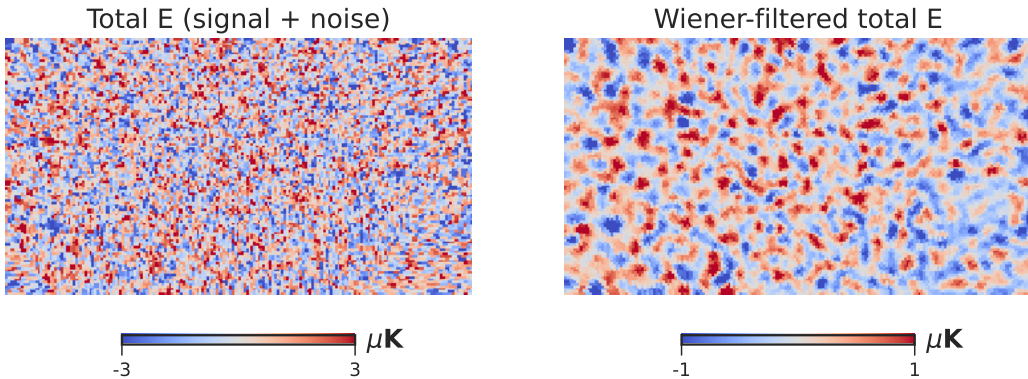


Figure 7. A satellite E-mode map with Planck-like noise before (left) and after (right) Wiener filtering. Note the difference in the color scale. For illustration purposes, this view is plotted at the same zoom/resolution as we did with the ground-based experiment patch in previous figures.

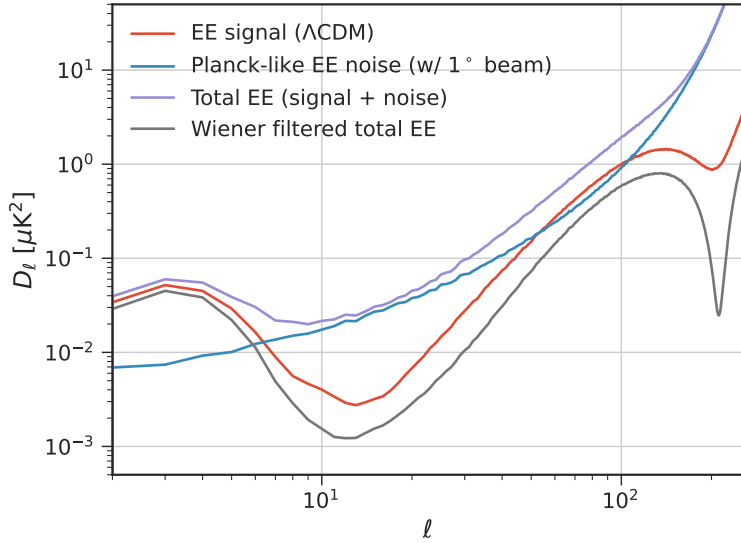


Figure 8. EE power spectrum of 128 TTEE simulations + Planck-like noise for the satellite E-mode map, before and after Wiener filtering. The Wiener filter is effective in removing noise and prevents overestimation of the leakage template.

3.3 Implementation: map-based E/B separation

We now have all the tools to perform map-based E/B separation. The first step is to estimate the leakage template by processing our Wiener-filtered satellite E-mode map through the ground-based experiment TOD filtering pipeline. The resulting leakage template includes both the partial-sky and filtering leakage. See Figure 9 for an example of the leakage templates estimated from Planck-like/LiteBIRD-like E-modes and the true leakage template. The estimated template is subtracted from the filtered ground-based experiment map in Q/U space to mitigate the E/B mixing.

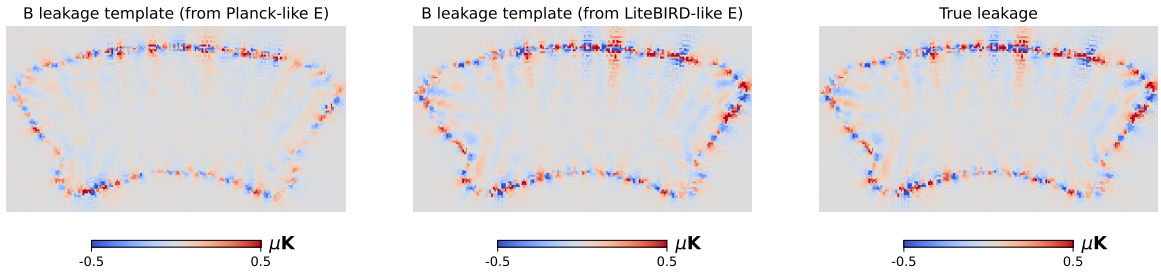


Figure 9. B map leakage templates as a result of observing the Wiener-filtered E-mode maps. The leakage along the boundary comes from the partial sky coverage, whereas the dimmer structure inside the patch comes from the TOD filtering. The leakage template estimated from LiteBIRD-like E-modes (middle) is close to the true leakage (right), where the Planck-like E-modes (left) underestimate the leakage.

To be explicit, the exact operation to perform map-based E/B separation is

$$\mathbf{m} = \mathbf{m}_{\text{obs}} - \mathbf{m}_{\text{obs}}^E \quad (3.5)$$

where \mathbf{m}_{obs} is the observed ground-based experiment Q/U map and $\mathbf{m}_{\text{obs}}^E$ is the leakage template in Figure 9 but in Q/U space. The leakage subtracted Q/U map is then passed to the power spectrum estimator, where KS purification is applied on top to tackle any residual leakage. We note that using KS purification in tandem with map-space leakage subtraction is not strictly necessary, and one can simply use the scalar-PCL method described in [11]. However, we have found that using both gives a slight edge in the results, which are discussed in Section 4.

4 Results

We explore the results in two parts. First, we evaluate the absolute value of the leakage for each mitigation method by looking at leakage B maps/BB spectra from TTEE simulations. Then, we compute the BB spectra from TTEE+BB simulations plus ground-based experiment noise to put the results into context. For example, even if the absolute level of leakage between two methods differ by an order of magnitude, the impact on the final sensitivity can be negligible if both residual leakages are significantly below the noise level. We compute the Fisher uncertainty $\sigma(r)$ on the TTEE+BB simulations as our final metric of merit.

4.1 Leakage maps and spectra (TTEE input)

Our three E/B separation cases of study are:

1. Residual B map/BB spectra of filtered TTEE input after leakage subtraction from Planck-like E-modes
2. Residual B map/BB spectra of filtered TTEE input after leakage subtraction from LiteBIRD-like E-modes
3. Residual B map/BB spectra of filtered TTEE input after matrix purification

We examine their residual leakage maps/spectra in Figure 10 and Figure 11, respectively.

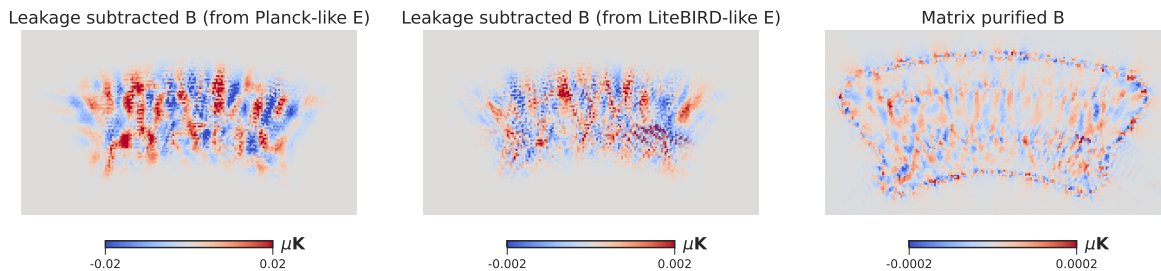


Figure 10. Residual apodized leakage B maps after leakage subtraction with Planck-like E-modes (left), LiteBIRD-like E-modes (middle), and matrix purification (right). Note the dramatically different color scales. The matrix purification significantly outperforms both leakage template subtraction methods in the absence of noise and B-mode input.

We see from the color scales of the leakage maps in Figure 10 that both map-space leakage subtraction and matrix purification are effective in reducing leakage (compared to the unmitigated leakage in Figure 9). Template subtraction with LiteBIRD-like E-modes reduce the map-space leakage by an order of magnitude compared to Planck-like E-modes,

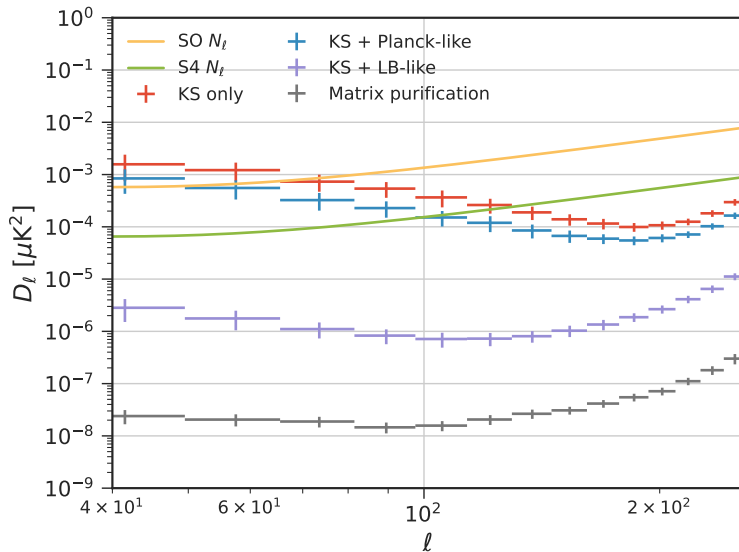


Figure 11. BB leakage spectra for 256 TTEE simulations corresponding to the residual leakage maps in Figure 10. Doing nothing to mitigate the TOD filtering leakage is labeled as “KS only” (red) while leakage subtraction with the corresponding E-modes are labeled as “KS + Planck/LB-like.” As with the residual leakage maps, the matrix purification method performs the best in terms of absolute level of leakage. However, the residual leakage of both leakage subtraction with LiteBIRD-like E-modes and matrix purification are comfortably below the noise even for the S4-like case.

and the matrix purification performs the best of the three methods by another order of magnitude. This is corroborated by the leakage spectra results in Figure 11.

A practical factor that may degrade the performance of the matrix purification compared to our idealistic simulation is the accuracy of the observation matrix. Our simulations use a short 24-hour observing schedule for convenience, which means the observation matrix can be computed exactly. In practice, the observation matrix is estimated over a subset of the observing season with scanning representative of the entire dataset. Another note is due to the steep scaling of computational resources with N_{side} , it is unlikely that the matrix purification can be done at the full resolution of the maps themselves. These factors are expected to have an impact visible on the scale of the leakage spectra in Figure 11. However, as previously discussed, the absolute level of leakage is not always the most relevant metric in the presence of noise and other residuals. Since the residual leakage of both leakage subtraction with LiteBIRD-like E-modes and matrix purification are far below the ground-based experiment noise levels (Figure 11), we expect both methods to perform similarly upon the inclusion of noise. In the next section, we will reevaluate the results in the presence of noise and lensing residuals.

4.2 Spectra with noise and lensing residuals (TTEE_{BB} input)

We now consider input BB spectra with SO/S4-like noise levels combined with 10% (nominal) and 1% (optimistic) lensing residuals, which arise from delensing in the presence of noise [6]. We assume foregrounds residuals are negligible and leave it for future work.

Figure 12 is the culmination of our results. We see that the E/B leakage due to TOD filtering starts to bias the spectra at low- ℓ , imparting significant additional variance. Leakage

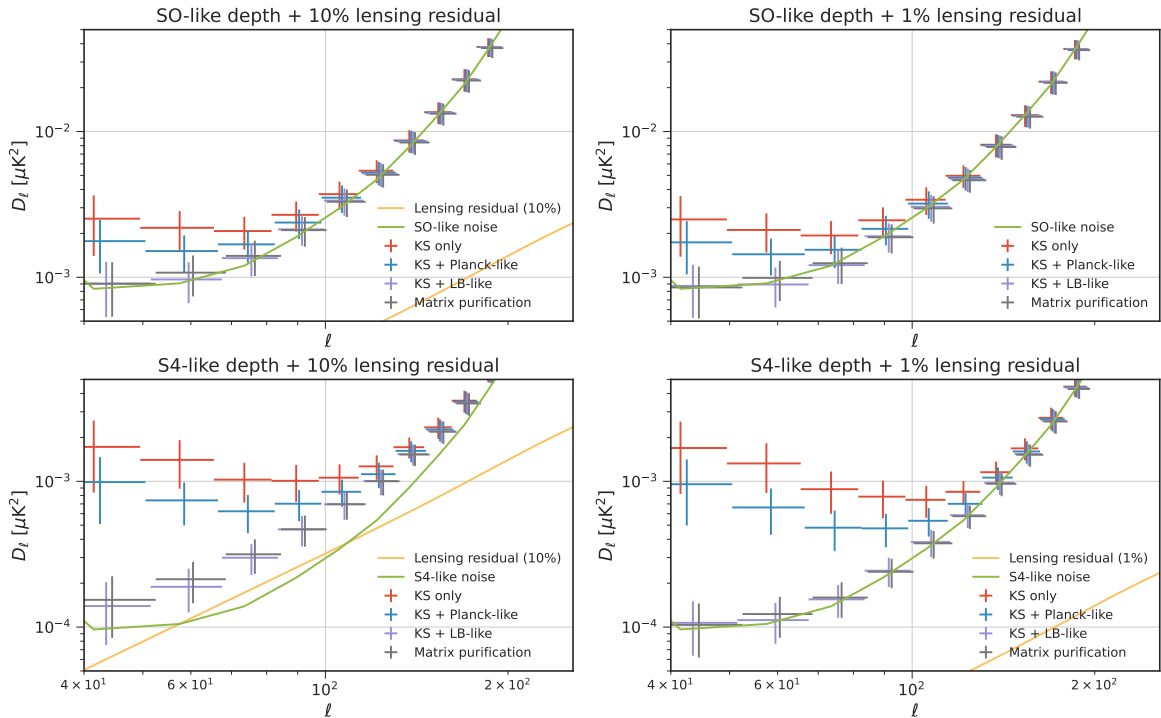


Figure 12. Reconstructed BB spectra (256 TTEEBB simulations) of different E/B separation techniques in the context of two different map depths and lensing residuals. E/B leakage due to TOD filtering elevates the spectra above the noise bias starting around $\ell = 100$. While the mean can be artificially debiased, the variance cannot, so we leave it in for illustration purposes. Each E/B separation technique can then be assessed on how close it brings the spectra back to the noise floor. A small $\Delta\ell = 1$ offset is applied among the flavors in each bin to avoid overlap.

subtraction with Planck-like E-modes does only slightly better compared to KS purification only, which is expected given Planck’s relatively high polarization noise. Leakage subtraction with LiteBIRD-like E-modes and matrix purification brings the spectra close to the noise floor once again. We see that despite the absolute level of leakage being orders of magnitude higher for the LiteBIRD-like case compared to the matrix purification, the difference ends up being negligible in the presence of noise and other residuals. To conclude our results, we propagate the spectra in Figure 12 to $\sigma(r = 0)$.

4.3 Fisher forecast for $\sigma(r = 0)$

We first write the observed B-mode spectrum following [19] (ignoring foregrounds and other systematics)

$$C_\ell^{BB,obs} = r \times C_\ell^{BB,prim}(r = 1) + C_\ell^{BB,lens} + C_\ell^{BB,noise} + C_\ell^{BB,leakage} \quad (4.1)$$

Given the likelihood \mathcal{L} from [20], the Fisher uncertainty $\sigma(r=0)$ can be written as

$$\sigma(r=0) \approx \left(\sqrt{\frac{\partial^2 \mathcal{L}}{\partial r^2} \Big|_{r=0}} \right)^{-1} \approx \frac{1}{\sqrt{\frac{f_{\text{sky}}}{2} \sum_{\ell} (2\ell + 1) \left(\frac{C_{\ell}^{BB, \text{prim}}(r=1)}{C_{\ell}^{BB, \text{lens}} + C_{\ell}^{BB, \text{noise}} + C_{\ell}^{BB, \text{leakage}}} \right)^2}} \quad (4.2)$$

The BB spectrum from $40 < \ell < 256$ of each independent MC in Figure 12 is used as the denominator in Equation 4.2, resulting in the histograms in Figure 13. The percent improvement of $\sigma(r)$ given an E/B separation method X over only using KS purification is defined as

$$\% \text{ improvement} = \frac{|\sigma(r)_{\text{median}}^X - \sigma(r)_{\text{median}}^{\text{KS}}|}{\sigma(r)_{\text{median}}^{\text{KS}}} \times 100 \quad (4.3)$$

and is shown for each method to the right of the arrow in Table 3 along with the summary statistics.

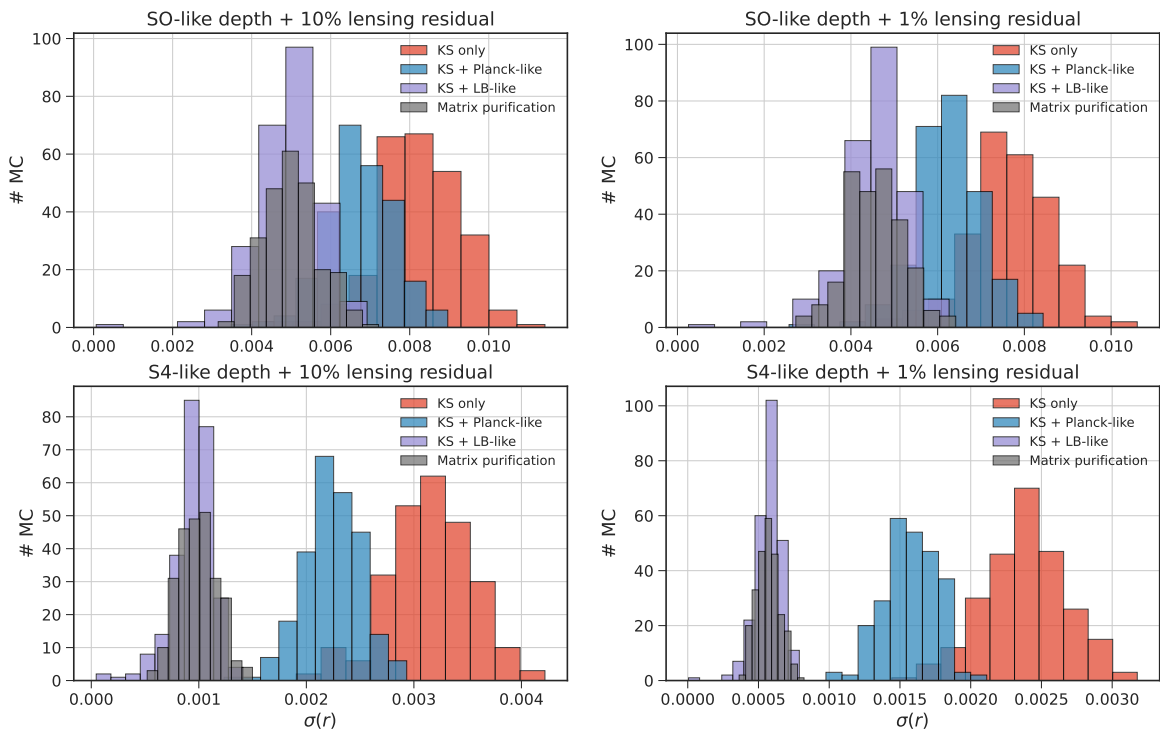


Figure 13. $\sigma(r)$ histograms of each BB spectra in Figure 12. Each E/B separation method improves upon $\sigma(r)$, shifting the histograms to the left. We note that the lower the noise/lensing residual, the bigger improvement each E/B separation method has. As already seen in Figure 12, KS + LiteBIRD-like E-modes performs essentially just as well as the matrix purification for these residuals, at a much lower computational cost. The statistics are summarized in Table 3.

Based on the percent improvement, we observe that cases with lower levels of residuals (such as S4-like depth + 1% lensing) benefit more from all E/B separation methods and vice-versa. This is the expected result when multiple residuals compete for critical path to optimal sensitivity, incentivizing us to carefully characterize our experiments.

Method	SO-like/10%	SO-like/1%	S4-like/10%	S4-like/1%
KS only	$8.2^{+1.0}_{-0.8}$	$7.7^{+0.9}_{-0.8}$	$3.1^{+0.4}_{-0.3}$	$2.4^{+0.3}_{-0.3}$
KS+Planck-like	$6.7^{+0.8}_{-0.8} \rightarrow 18\%$	$6.3^{+0.7}_{-0.7} \rightarrow 18\%$	$2.2^{+0.3}_{-0.2} \rightarrow 29\%$	$1.6^{+0.2}_{-0.2} \rightarrow 33\%$
KS+LiteBIRD-like	$5.0^{+0.6}_{-0.9} \rightarrow 38\%$	$4.6^{+0.6}_{-0.6} \rightarrow 40\%$	$0.96^{+0.2}_{-0.2} \rightarrow 69\%$	$0.58^{+0.07}_{-0.1} \rightarrow 76\%$
Matrix purification	$5.0^{+0.8}_{-0.7} \rightarrow 39\%$	$4.5^{+0.7}_{-0.6} \rightarrow 41\%$	$0.99^{+0.2}_{-0.2} \rightarrow 68\%$	$0.56^{+0.09}_{-0.08} \rightarrow 76\%$

Table 3. $\sigma(r) \times 10^3$ medians with 68% percentile intervals of each histogram in Figure 13. Rows correspond to E/B separation methods and columns correspond to the combination of a ground-based experiment noise level plus a lensing residual percentage. Improvement over KS only for a method X is defined in Equation 4.3 and displayed to the right of the arrow in each cell. We note again that each E/B separation technique has an increasing factor of improvement with decreasing residual noise/lensing.

5 Discussion

We have shown that the map-based E/B separation method via leakage template subtraction is effective in reducing $\sigma(r)$ by mitigating the E/B leakage due to TOD filtering. The absolute effectiveness is dependent on the depth of the E-modes used to estimate the leakage template, while the relative effectiveness compared to only using KS purification depends on the level of residuals present in the map.

In terms of absolute level of leakage mitigation, the matrix purification technique outperforms even leakage subtraction using LiteBIRD-like E-modes by two orders of magnitude (see discussion in Section 4.1). However, since both levels of leakage are well below the noise levels of even the S4-like patch, they end up performing very similarly.

Considering the near future, experiments such as SO may be able to benefit from leakage subtraction using Planck E-mode maps by around 10-20% in $\sigma(r)$ over using KS purification only, although we stress once again that our improvement factors in Table 3 are not meant to be a realistic forecast. Either way, we recommend that the matrix purification method be utilized if computational resources allow as it vastly outperforms Planck E-modes in all cases. However, if there happen to be additional systematics that increase the effective noise, we could be in a scenario in which we cannot reap the full benefits of the matrix purification. In that case, one would have to decide whether the computational challenges are worth the benefits.

Since the cost of implementing matrix purification will only increase as ground-based experiments deploy more detectors (see discussion of scaling in Section 2.4), we imagine map-space leakage subtraction will become a much more attractive alternative once LiteBIRD (or similar depth) maps are available. The E/B separation performance is on par with matrix purification even at S4-like depths at a small fraction of the computational cost.

5.1 Future work

We take the opportunity to discuss several avenues for improving upon the results in this paper:

- Generate a more realistic observing schedule/patch geometry for forecasting. Use a subset of the observing schedule to compute the observation matrix and study the effect on matrix purification. We used a simple 24-hour schedule and a fixed patch for all experiments for simplicity, which allowed exact computation of the observation matrix.

- Include foregrounds residuals as another source of C_ℓ^{BB} , although this will involve the need to consider different observing frequencies.
- Use the Planck NPIPE2020⁶ simulation maps to properly evaluate map-based E/B separation with Planck E-modes. Here, we simply generated isotropic noise for easier direct comparison with the LiteBIRD-like case.
- Study the effect of instrumental systematics between ground-based and satellite experiments, such as calibration mismatch. While ground-based experiments calibrate off of satellite experiments for their absolute gain, differences in relative gain will impact map-space combinations.

6 Conclusion

E/B leakage due to TOD filtering is and will continue to be a critical source of sensitivity loss to mitigate for both current and future ground-based CMB experiments. However, the current standard of matrix purification may prove to be computationally challenging to scale into the future. We have presented an alternate method based on [11] in which a leakage template is estimated from satellite E-modes and subtracted from ground-based experiment maps. The method was evaluated with a full TOD simulation for the ground-based experiment and compared to the existing matrix purification technique. We found that leakage subtraction with LiteBIRD-like E-modes and matrix purification perform very similarly for all cases of interest, with Planck-like E-modes lagging farther behind. As future experiments produce deeper E-mode maps, we expect to see map-based E/B separation become more mainstream due to its simplicity, high performance, and low computational cost.

A Implementation: matrix purification

We briefly describe our implementation of the matrix purification for completeness. We follow the procedure in [8, 21] with slight adjustments.

The first step is to generate analytic signal covariance matrices \mathbf{C}_E and \mathbf{C}_B with a $1/\ell^2$ spectrum following [17]. We expedite the process by only considering the observed pixels in the hit map (Figure 3). The observation matrix \mathbf{R} with the selected observing schedule and filter stack is generated by TOAST and apodized with NaMaster

$$\mathbf{R} = \mathbf{Z}\mathbf{R}_{\text{unapo}} \quad (\text{A.1})$$

where \mathbf{Z} is the diagonal apodization matrix. The signal covariance is observed with \mathbf{R} as per Equation 2.10. The generalized eigenvalue problem in Equation 2.9 is

$$(\tilde{\mathbf{C}}_B + \sigma^2\mathbf{I})\mathbf{x}_i = \lambda_i(\tilde{\mathbf{C}}_E + \sigma^2\mathbf{I})\mathbf{x}_i \quad (\text{A.2})$$

where we perturb $\tilde{\mathbf{C}}_{E/B}$ with a small regularization factor σ (and \mathbf{I} is the identity) to make the problem positive semi-definite. The factor σ needs to be large enough that the eigenvalue problem is numerically solvable, but not so large as to significantly perturb the generalized eigenvectors. We follow the BICEP/Keck collaboration’s convention and set σ to be 0.1% of the mean of the diagonal of $\tilde{\mathbf{C}}$. The upper half of the solved eigenvalue spectrum and the two extrema eigenvectors of our set are plotted in Figure 14 and Figure 15, respectively.

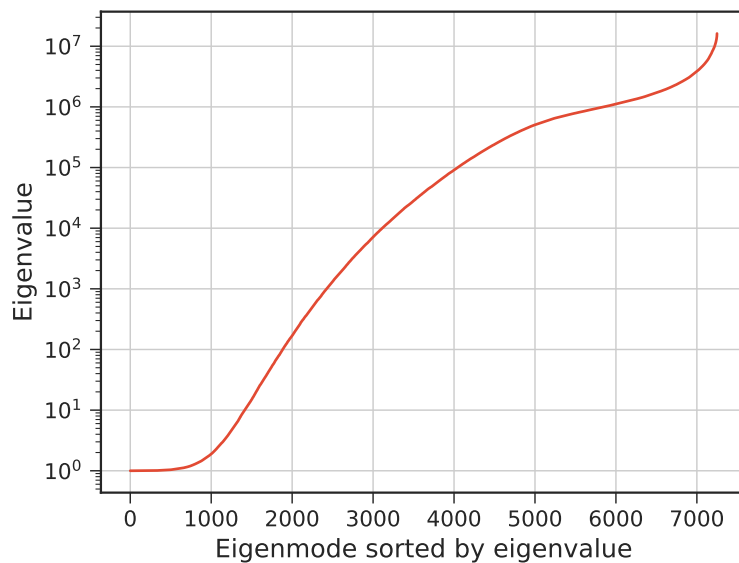


Figure 14. Largest 7250 eigenvalues of the generalized eigenvalue problem (Equation 2.9). Eigenmodes with larger eigenvalues are associated with more pure B-modes as per Equation 2.11.

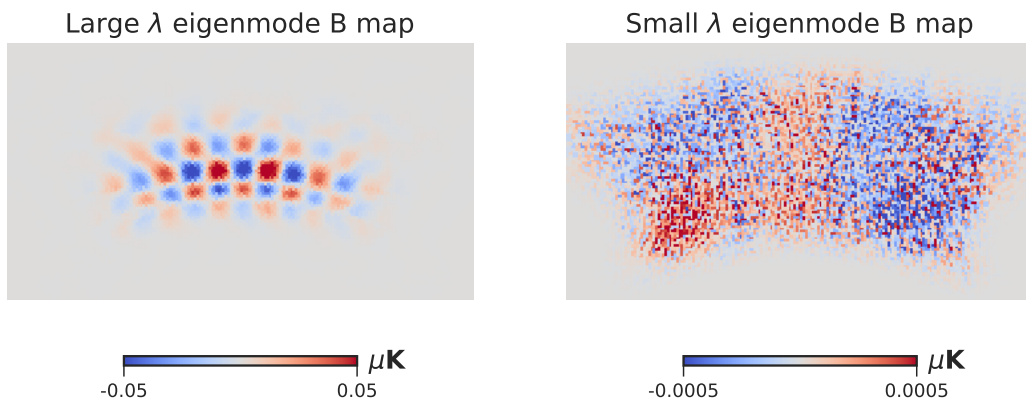


Figure 15. Apodized eigenvectors with the largest eigenvalue (left) and the smallest eigenvalue (right) in our set, corresponding to the most “pure” B-mode and the most “ambiguous” mode in our set, respectively. We observe that the purer B-modes primarily manifest in low- ℓ power whereas more ambiguous modes contain more high- ℓ power.

Finally, the purification matrix is constructed via Equation 2.12. We approximate the BICEP convention and use eigenvectors with $\lambda \geq 1.02$ to construct the purification matrix. The matrix purified map is then just the product of the purification matrix with an observed map, as in Equation 2.13.

Acknowledgments

This work is supported by the Simons Array experiment funded by grants from the Simons Foundation, the Gordon and Betty Moore Foundation, the Templeton Foundation, the Na-

⁶<https://portal.nersc.gov/project/cmb/planck2020/>

tional Science Foundation, and the International Center for Quantum-field Measurement Systems for Studies of the Universe and Particles (QUP). Special thanks to Reijo Keskitalo of Lawrence Berkeley National Laboratory’s Computational Cosmology Center for providing software support and observation matrix estimates. Lastly, we thank Josquin Errard for Fisher forecast discussions, Akito Kusaka for draft comments, and Radek Stompor for useful references.

References

- [1] D.J. Fixsen, E.S. Cheng, J.M. Gales, J.C. Mather, R.A. Shafer and E.L. Wright, *The cosmic microwave background spectrum from the fullcobefiras data set*, *The Astrophysical Journal* **473** (1996) 576–587.
- [2] C.L. Bennett, D. Larson, J.L. Weiland, N. Jarosik, G. Hinshaw, N. Odegard et al., *Nine-year wilkinson microwave anisotropy probe (wmap) observations: Final maps and results*, *The Astrophysical Journal Supplement Series* **208** (2013) 20.
- [3] Planck Collaboration, N. Aghanim, Y. Akrami, F. Arroja, M. Ashdown, J. Aumont et al., *Planck 2018 results. I. Overview and the cosmological legacy of Planck*, *aap* **641** (2020) A1 [1807.06205].
- [4] U. Seljak and M. Zaldarriaga, *Signature of gravity waves in the polarization of the microwave background*, *Physical Review Letters* **78** (1997) 2054–2057.
- [5] E. Hivon, K.M. Gorski, C.B. Netterfield, B.P. Crill, S. Prunet and F. Hansen, *Master of the cosmic microwave background anisotropy power spectrum: A fast method for statistical analysis of large and complex cosmic microwave background data sets*, *The Astrophysical Journal* **567** (2002) 2–17.
- [6] K.N. Abazajian, P. Adshead, Z. Ahmed, S.W. Allen, D. Alonso, K.S. Arnold et al., *Cmb-s4 science book, first edition*, 2016. 10.48550/ARXIV.1610.02743.
- [7] The Polarbear Collaboration, S. Adachi, M.A.O.A. Faúndez, K. Arnold, C. Baccigalupi, D. Barron et al., *A measurement of the degree-scale cmb b-mode angular power spectrum with polarbear*, *The Astrophysical Journal* **897** (2020) 55.
- [8] P.A.R. Ade, Z. Ahmed, R.W. Aikin, K.D. Alexander, D. Barkats, S.J. Benton et al., *Bicep2/keck array. vii. matrix based e/b separation applied to bicep2 and the keck array*, *The Astrophysical Journal* **825** (2016) 66.
- [9] N. Goeckner-Wald, R. Keskitalo, Y. Chinone, P.A. Gallardo, A. Kusaka, A.T. Lee et al., *Designs for next generation cmb survey strategies from chile*, in *Millimeter, Submillimeter, and Far-Infrared Detectors and Instrumentation for Astronomy IX*, J. Zmuidzinas and J.-R. Gao, eds., p. 136, SPIE, July, 2018, DOI.
- [10] P. Ade, J. Aguirre, Z. Ahmed, S. Aiola, A. Ali, D. Alonso et al., *The simons observatory: science goals and forecasts*, *Journal of Cosmology and Astroparticle Physics* **2019** (2019) 056–056.
- [11] S. Ghosh, J. Delabrouille, W. Zhao and L. Santos, *Towards ending the partial sky e-b ambiguity in cmb observations*, *Journal of Cosmology and Astroparticle Physics* **2021** (2021) 036–036.
- [12] E. Allys, K. Arnold, J. Aumont, R. Aurlien, S. Azzoni, C. Baccigalupi et al., *Probing cosmic inflation with the litebird cosmic microwave background polarization survey*, *Progress of Theoretical and Experimental Physics* **2023** (2022) .
- [13] E.F. Bunn, M. Zaldarriaga, M. Tegmark and A. de Oliveira-Costa, *E/bdecomposition of finite pixelized cmb maps*, *Physical Review D* **67** (2003) .

- [14] K.M. Smith, *Pseudo- C_ℓ estimators which do not mix e and b modes*, *Phys. Rev. D* **74** (2006) 083002.
- [15] J. Grain, M. Tristram and R. Stompor, *Polarized cmb power spectrum estimation using the pure pseudo-cross-spectrum approach*, *Phys. Rev. D* **79** (2009) 123515.
- [16] D. Alonso, J. Sanchez and A. Slosar, *A unified pseudo- c_ℓ framework*, *Monthly Notices of the Royal Astronomical Society* **484** (2019) 4127–4151.
- [17] M. Tegmark and A. de Oliveira-Costa, *How to measure cmb polarization power spectra without losing information*, *Physical Review D* **64** (2001) .
- [18] T. Kisner, R. Keskitalo, A. Zonca, J.R. Madsen, J. Savarit, M. Tomasi et al., *hpc4cmb/toast: Update pybind11*, Oct., 2021. 10.5281/zenodo.5559597.
- [19] J. Errard, *Habilitation à diriger des recherches*, 2024.
- [20] M. Tegmark, A.N. Taylor and A.F. Heavens, *Karhunen-loeve eigenvalue problems in cosmology: How should we tackle large data sets?*, *The Astrophysical Journal* **480** (1997) 22–35.
- [21] J. Willmert, *Constraining Inflationary B-modes with the BICEP/Keck Array Telescopes*, phd thesis, University of Minnesota Twin Cities, November, 2019.